ChemistryOpen

Research Article
doi.org/10.1002/open.202200110

Chemistry Europe
European Chemical Societies Publishing

www.chemistryopen.org

An Activatable ^{19}F MRI Molecular Probe for Sensing and Imaging of Norepinephrine

Lingxuan Li[+], Ao Li[+], Yaying Lin, Dongxia Chen, Bilun Kang, Hongyu Lin,* and Jinhao Gao*[a]

Norepinephrine (NE), acting as both a neurotransmitter and hormone, plays a significant role in regulating the action of the brain and body. Many studies have demonstrated a strong correlation between mental disorders and aberrant NE levels. Therefore, it is of urgent demand to develop *in vivo* analytical methods of NE for diagnostic assessment and mechanistic investigations of mental diseases. Herein, we report a ^{19}F MRI probe (**NRFP**) for sensing and imaging NE, which is constructed by conjugating a gadolinium chelate to a fluorine-containing moiety through a NE-responsive aromatic thiocarbonate linkage. The capacity and specificity of **NRFP** for detecting NE is validated with *in vitro* detecting/imaging experiments. Furthermore, the feasibility of **NRFP** for visualizing NE in animals is illustrated by *ex vivo* and *in vivo* imaging experiments, demonstrating the promising potential of **NRFP** for selective detection and specific imaging of NE in deep tissues of living subjects.

Introduction

Norepinephrine (NE), a crucial neurotransmitter and hormone in vertebrates, plays a fundamental role in various physiological processes to maintain the homeostasis and facilitate the tackling of various changes during metabolism.[1–3] NE is synthesized by a series of enzymatic reactions starting from L-tyrosine with levodopa and dopamine (DA) as the intermediates, which can be further converted to epinephrine (E) in the neurons of the locus coeruleus (LC) in the brain (Figure 1a).[4] In biological systems, NE is critical for nervous system development, memory refreshment, heart rate regulation and blood pressure stabilization.[3,5–6] It is generally accepted that there is a strong correlation between abnormal metabolic levels of NE and psychiatric conditions or neurodegenerative diseases.[7–10] In recent decades, with the rapid pace of modern life and the increased pressure it brings, the number of people who are suffering from mental disorders such as depression has exceeded more than 260 million all around the world. Many studies concentrating on depression have demonstrated that this disease is mainly related to the decreased levels of NE in the brain.[11–12] Though the interactions between NE and its receptors usually lasts for a very short period of time, they are capable of exerting a wide range of effects to the body for several hours or even days. Therefore, *in vivo* detection of NE is of great importance for sensitive diagnostic assessment and in-depth mechanistic studies of mental disorders such as depression. Traditional methods, like electrochemical analysis and mass spectrometry, have been widely used for detection and measurement of neurotransmitters in organism. However, they are facing substantial challenges for *in vivo* analysis and sensing.[12–13] Recently, a variety of fluorescence probes for depression assessment based on detecting neurotransmitter in complex physiological environments have been reported.[14–16] Unfortunately, several obstacles need to be overcome for the further applications of these approaches, which include the shallow tissue penetration of fluorescence and the low specificity towards NE due to the structural similarity of three catecholamine neurotransmitters (DA, NE, and E).[12]

Among different molecular imaging techniques, magnetic resonance imaging (MRI) has attracted significant attention from researchers for its advantages of deep penetration, high resolution, non-ionizing radiation, and multi-parameter imaging.[17–19] As a real-time and deep-tissue imaging method, ^{1}H MRI is widely used in clinic, which is rendering the difference in relaxation time for protons in various soft tissues,[20] and therefore offering high-resolution anatomical images for diagnosis.[21–22] Nevertheless, the interferences from high background and artifacts obstruct the application of ^{1}H MRI for detecting bioactive molecules in organisms that are of relatively low concentration.[23–24] ^{19}F, which is of 100% natural abundance, a wide range of chemical shifts, a gyromagnetic ratio close to ^{1}H (94% relative to ^{1}H),[25] is regarded as an ideal type of nuclei complementary to ^{1}H for MRI. Most importantly,[26–27] the ^{19}F content in the human body is extremely low ($< 10^{-6}$ M),[28–29] which allows ^{19}F MRI to detect low concentration species with negligible background and render their distributions as "hot-spot" images.[30–36] Therefore, ^{19}F MRI is gaining momentum in the field of sensing and imaging low concentration bioactive species.[37–47]

[a] *L. Li,[+] Dr. A. Li,[+] Y. Lin, D. Chen, B. Kang, Dr. H. Lin, Prof. Dr. J. Gao*
The MOE Laboratory of Spectrochemical Analysis & Instrumentation
Fujian Provincial Key Laboratory of Chemical Biology,
and Department of Chemical Biology,
College of Chemistry and Chemical Engineering
Xiamen University
Xiamen 361005 (P. R. China)
E-mail: hylin007@xmu.edu.cn
jhgao@xmu.edu.cn

[+] *These authors contributed equally to this work.*

Supporting information for this article is available on the WWW under https://doi.org/10.1002/open.202200110

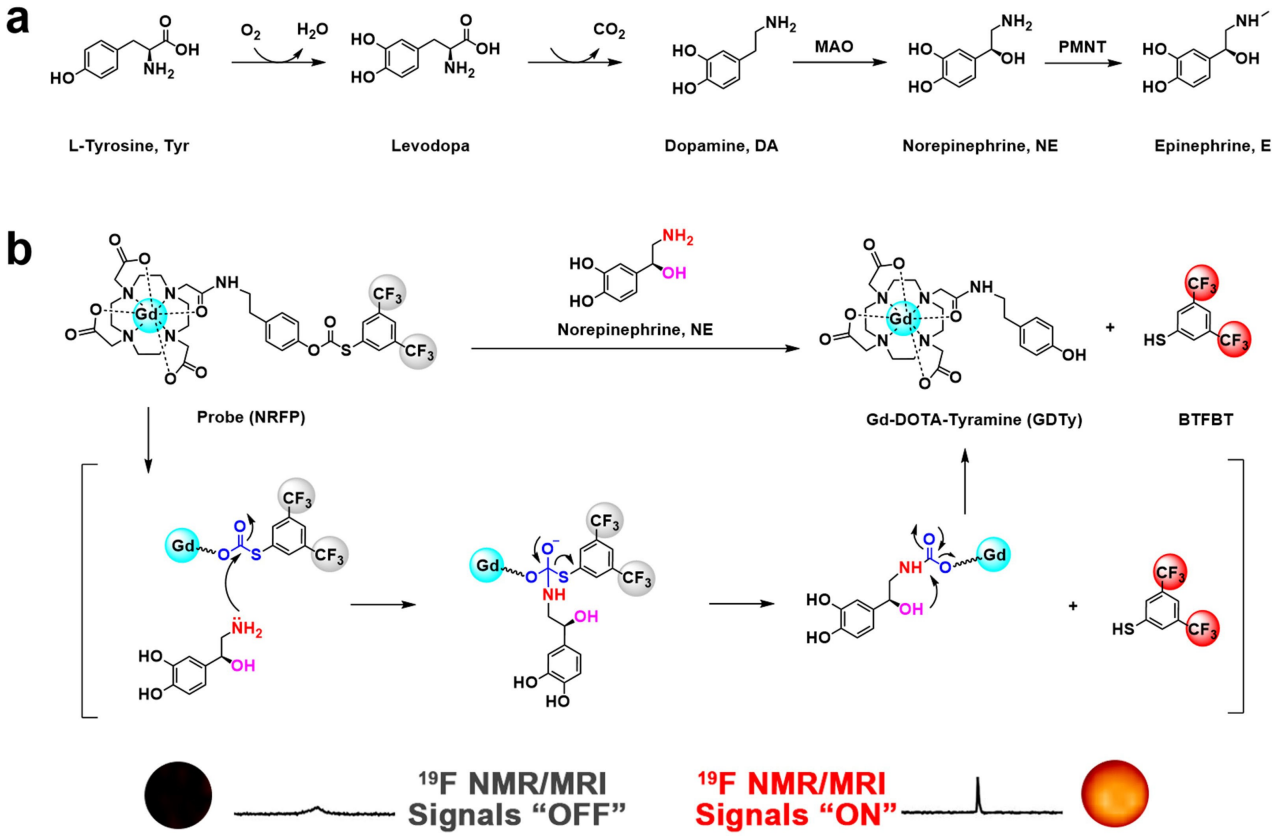

Figure 1. (a) *In vivo* metabolic pathways of catecholamines, including dopamine (DA), norepinephrine (NE), and epinephrine (E). MAO: monoamine oxidase; PMNT: phenylethanolamine *N*-methyltransferase. (b) A schematic illustration showing the functional mechanism of our norepinephrine-responsive ^{19}F MRI probe (**NRFP**). ^{19}F NMR/MRI signals of **NRFP** are "OFF" due to the strong paramagnetic relaxation enhancement (PRE) effect exerted by the chelated Gd^{3+} ion. The effect is significantly weakened when norepinephrine (NE) selectively cleaves the aromatic thiocarbonate linkage, which releases 3,5-bis(trifluoromethyl)benzene-thiol (BTFBT), leading to the switching "ON" of ^{19}F NMR/MRI signals.

In light of these considerations, we envision that detecting NE with ^{19}F MRI might offer a potential means to circumvent the obstacles encountered by fluorescent approaches. We design a norepinephrine-responsive ^{19}F MRI probe (**NRFP**) by linking a Gd chelate (Gd-DOTA) to a fluorine-containing small molecule 3,5-bis(trifluoromethyl)benzenethiol (BTFBT) *via* an aromatic thiocarbonate linkage, which is specifically responsive to NE. In **NRFP**, because of the paramagnetic relaxation enhancement (PRE) effect exerted by the Gd chelate,[48] the longitudinal and transverse relaxation times (T_1 and T_2) of ^{19}F nuclei in BTFBT are significantly shortened, resulting in the "OFF" state of ^{19}F signals.[49] Once NE cleaves the aromatic thiocarbonate linkage and releases BTFBT from **NRFP**, the PRE effect is substantially attenuated due to the increased distance between the Gd chelate and BTFBT, leading to the recovery of the relaxation times and the "ON" state of ^{19}F signals (Figure 1b), which allows for the detection and imaging of NE.[50] We quickly validate the working principle of the probe by measuring the T_1 and T_2 of ^{19}F before and after **NRFP**'s response to NE. Additionally, we illustrate the feasibility and specificity of **NRFP** for the detection and imaging of NE *via in vitro* detecting/imaging experiments. Finally, we achieve *ex vivo* and *in vivo* imaging of NE by ^{19}F MRI with **NRFP**, demonstrating the promising potential of our probe for selective detection and specific imaging of NE in the deep tissues of living subjects.

Results and Discussion

Synthesis of NRFP

NRFP was synthesized in a facile and modular approach (Scheme S1, Supporting Information). Briefly, we first synthesized Compound **3**, which serves as a moiety to chelate Gd^{3+} in **NRFP**. 3,5-Bis(trifluoro-methyl)benzenethiol (BTFBT), which serves as a fluorine-bearing moiety in **NRFP** was then coupled to **3** through a NE-responsive aromatic thiocarbonate linkage to afford Ligand **7**. The synthetic protocols and characterization data for compounds **1**–**7** are included in the Experimental Section and the Supporting Information. Chelation of **7** with Gd^{3+} ions afforded the final probe **NRFP** (**8**), which was confirmed by high-resolution mass spectrometry (HR-MS). The broad and short peak in the ^{19}F nuclear magnetic resonance (NMR) spectrum of **NRFP** indicates the significant PRE effect within the probe.

Measurements of ^{19}F Relaxation Times

We then measured the longitudinal and transverse relaxation times (T_1 and T_2) of ^{19}F in **NRFP** on a NMR spectrometer (564 MHz for ^{19}F). As shown in Table S1, the T_1 and T_2 of ^{19}F in **NRFP** were substantially shortened (less than 10 ms) compared to those in **7** (1287.0 and 787.8 ms, respectively), confirming the pronounced PRE effect with **NRFP**. Upon incubation with NE, the T_1 and T_2 of ^{19}F were considerably extended (to 621.0 and 232.2 ms, respectively), indicating the significant weakening of the PRE effect. These results confirm our design of **NRFP** and illustrate the feasibility of our probe for NE detection.

In vitro Sensing of NE with NRFP using ^{19}F NMR Spectroscopy

We further explored the detection of NE with **NRFP** *in vitro* by ^{19}F NMR. **NRFP** was incubated with NE and the reaction was monitored by ^{19}F NMR spectroscopy. The intensity of the peak in ^{19}F NMR spectra increased along with the extension of incubation time and reached a plateau after 60 min (Figure S1a), which is affirmed with signal-to-noise ratio (SNR) analysis (Figure S1b). This response was not affected by different pH conditions (Figure S2a). However, without NE, the intensity of the peak in ^{19}F NMR spectra remained low even after 48 h incubation (Figure S2b) or under different pH conditions (Figure S2c). These results indicate the successful response of **NRFP** to NE. We then studied the specificity of our probe. **NRFP** were incubated with a panel of analytes and the reactions were monitored by ^{19}F NMR. As shown in Figure 2a, **NRFP** did not respond to common biomolecules such as glucose and those in FBS, reducing agents such as glutathione (GSH), active sulfur substances such as L(+)-cysteine and homocysteine, or reactive oxygen species/reactive nitrogen species (ROS/RNS) such as alkylperoxy radicals ($RO^{\bullet}$), hydrogen peroxide (H_2O_2), hypochlorous acid (HClO) and peroxynitrite ($ONOO^-$). **NRFP** did respond to epinephrine and dopamine, but the responding efficiencies were insignificant compared to that of **NRFP** to NE. These observations are confirmed with SNR analysis (Figure 2b), indicating the excellent selectivity of **NRFP** for the detection of NE with a limit of detection (LOD) of 2.1 mM in ^{19}F NMR (Figure S3). We also investigated the response of **NRFP** to NE by high-performance liquid chromatography (HPLC). Incubation of **NRFP** with NE resulted in two new peaks in the HPLC chromatogram (Figure 2c), which were confirmed to be corresponding to the expected products Gd-DOTA-Tyramine (GDTy) and BTFBT (Figure 1b), respectively. These results indicate the successful and specific response of **NRFP** towards NE, which allows for selective detection of NE by ^{19}F NMR.

In vitro Imaging of NE using ^{19}F MRI with NRFP

We next investigated the imaging of NE by ^{19}F MRI with **NRFP**. A series of solutions containing **NRFP** at indicated concentrations were imaged on a 9.4 T MRI scanner with commercially available $^{1}H/^{19}F$ MRI coils before and after incubation with excess NE. The solutions showed no ^{19}F MRI signals before incubation with NE. In contrast, after incubation, these solutions exhibited significant signals, which intensified as the increase of **NRFP** concentration (Figure 3a). The specificity of **NRFP** was also evaluated. Incubation of **NRFP** with common bioactive molecules (glucose, GSH, and H_2O_2) showed no ^{19}F MRI signals while much stronger signals were observed for **NRFP** incubated with NE (Figure 3b). Incubation of **NRFP** with dopamine or epinephrine also showed some signals, but the intensities of these signals were relatively weak compared to those of **NRFP** incubated with NE. SNR analysis further confirms the significant enhancement in signal intensity for **NRFP** after incubation with NE, the positive correlation between signal intensity after response and **NRFP** concentration, and the specific response of **NRFP** towards NE. These results demonstrate that it is feasible to image NE with **NRFP** by ^{19}F MRI.

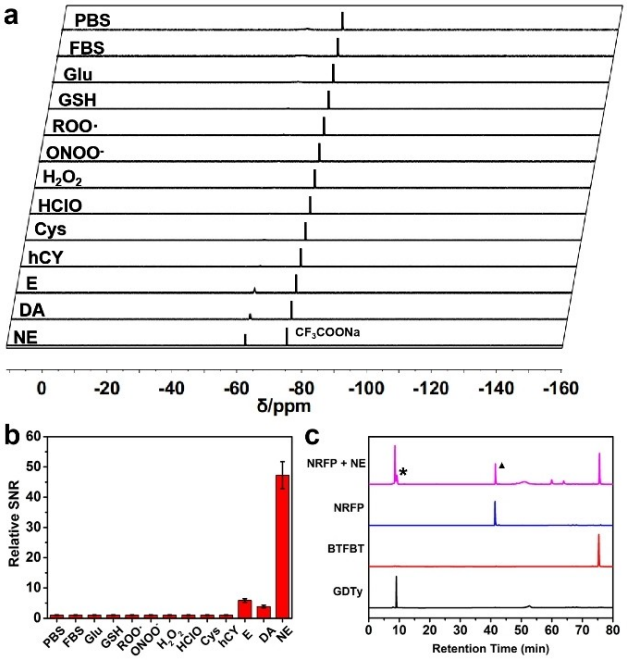

Figure 2. (a) Representative ^{19}F NMR spectra of **NRFP** (−62.7 ppm) in 500 μL 10% D_2O/H_2O (final concentration: 0.4 mM), which were incubated with various analytes for 3 h at 25 °C. PBS: 50 mM, pH 7.4; FBS: 10% in PBS; dopamine (DA), norepinephrine (NE) and epinephrine (E): 10 mM in PBS; Glu: 5.0 mM glucose in PBS; GSH: 2.0 mM glutathione in PBS; all other analytes: 0.40 mM in PBS for 3 h at 25 °C. CF_3COONa (at −75.4 ppm) was used as an internal reference. (b) Signal-to-noise ratio (SNR) analysis on the results of the experiment as indicated in (a) (n = 5). The SNR for the peak of **NRFP** in PBS was set as 1.0 and the other SNRs were normalized accordingly. (c) HPLC chromatograms showing **NRFP** (0.2 mM) alone and the products of **NRFP** incubated with 50 equiv. NE for 3 h. The expected products, Gd-DOTA-Tyramine (GDTy) and 3,5-bis(trifluoromethyl)benzene-thiol (BTFBT) were also analyzed. See Figure **S4** for HR-ESI-MS analysis of the fractions corresponding to the peaks indicated by an *asterisk* and a *triangle*.

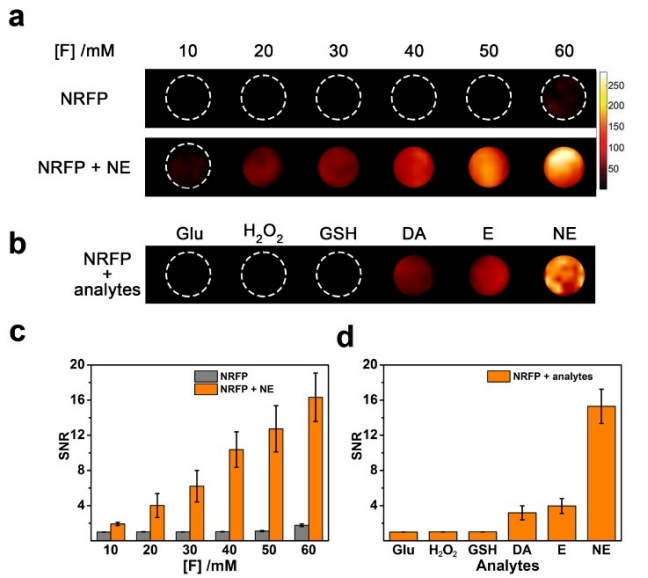

Figure 3. (a) Representative ^{19}F MR images of **NRFP** (at indicated concentrations) before and after specific activation towards NE (0.3 M). (b) Representative ^{19}F MR images of **NRFP** (60 mM ^{19}F) before and after incubated with: dopamine (DA), norepinephrine (NE) and epinephrine (E): 0.3 M in PBS; glucose (Glu), H_2O_2 and glutathione (GSH): 10 mM in PBS for 3 h at 25 °C. (c) SNR analysis on the results of the experiment as indicated in (a) (n = 5). The SNR for the ^{19}F MR image of 0.83 mM **NRFP** (i.e., 10 mM ^{19}F) in PBS was set as 1.0 and the other SNRs were normalized accordingly. (d) SNR analysis on the results of the experiment as indicated in (b) (n = 5). The SNR for the ^{19}F MR image of **NRFP** with glucose in PBS was set as 1.0 and the other SNRs were normalized accordingly.

Ex vivo Imaging of NE by ^{19}F MRI with NRFP

Before imaging experiments on animals, we quickly assessed the biocompatibility of **NRFP**. **NRFP** did not show significant cytotoxicity to L02 or HepG2 cells even at 20 mM (Figure S5a). No appreciable microscopic lesions were observed for hematoxylin and eosin (H&E) stained tissue section of all major organs collected from the mice at 7 d after intravenous injection of **NRFP** (Figure S5b). These results indicate the good biocompatibility of **NRFP**, which permits further imaging experiment on animals. We firstly performed imaging experiments with porcine muscle tissues. **NRFP** was subcutaneously injected to two different spots of a piece of pork, one of which was then further injected with NE (Figure 4a). The two sites of injection could be clearly seen in ^{1}H MRI images due to the Gd chelate in **NRFP**, which could act as a T_1 contrast agent, leading to signal enhancement of nearby tissues (Figure 4b). As revealed by ^{19}F MRI (Figure 4b), the tissues injected with **NRFP** and NE showed strong signals, the intensity of which peaked at 60 min after injection and decreased gradually. In contrast, no significant signals were observed for the tissues injected with **NRFP** alone. There observations are further confirmed by SNR analysis (Figure 4c). These results illustrate the feasibility of imaging NE in deep tissues by ^{19}F MRI with **NRFP**.

In vivo Imaging of NE *via* ^{19}F MRI with NRFP

Encouraged by the promising results of *ex vivo* imaging experiments, we further investigated the *in vivo* imaging of NE

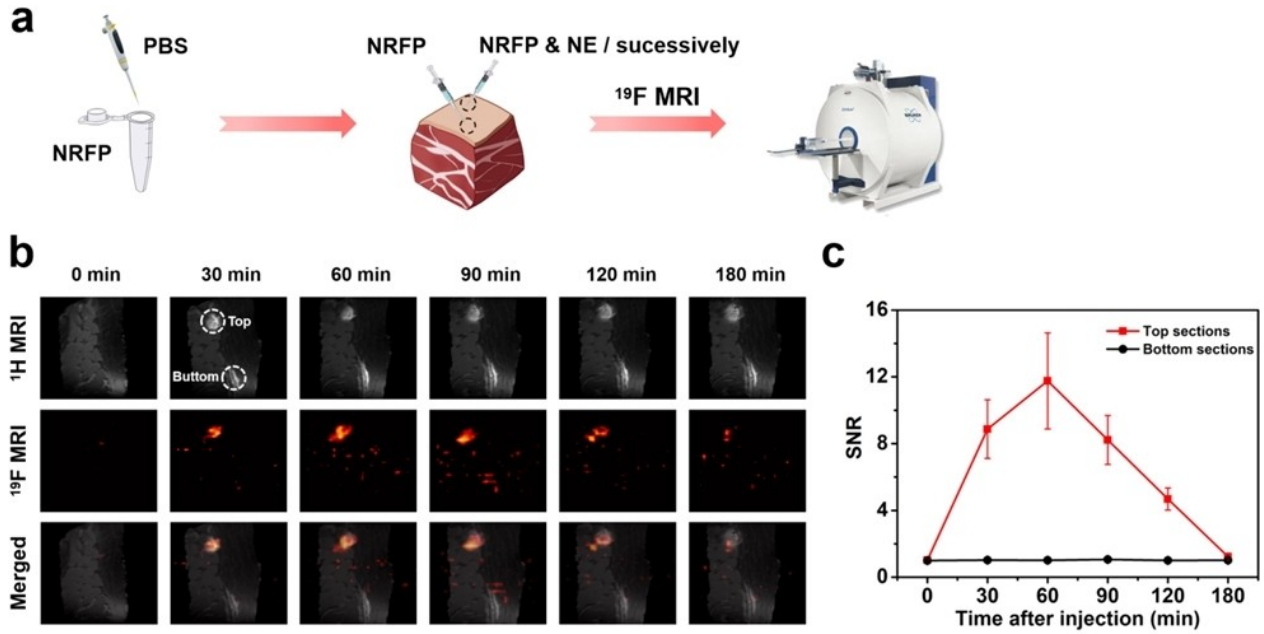

Figure 4. (a) A schematic illustration showing the protocol for *ex vivo* ^{19}F MRI. The center frequency corresponding to the ^{19}F chemical shift at −62.7 ppm was chosen for ^{19}F MRI. (b) Representative ^{1}H and ^{19}F MR images of a piece of pork at pre-injection (0 min) or indicated time points after subcutaneous injection of prepared **NRFP** solutions (200 μL), which were 10 mM **NRFP** in 1 × PBS incubated with 50 equiv. NE (Top) and 10 mM **NRFP** in 1 × PBS alone (Bottom). The sites of injection are indicated by white circles. (c) SNR analysis on the results of the experiment as indicated in (b) (n = 3). The SNR for the ^{19}F MR image of **NRFP** without NE treatment at 0 min was set as 1.0 and the other SNRs were normalized accordingly.

with **NRFP**. The left hinder limbs of BALB/c mice were injected with a solution of **NRFP** and the right hinder limbs were injected with a solution of **NRFP** and NE. Then the mice were subjected to MRI (Figure 5a). Due to the contrast-enhancing effect of the Gd chelate in **NRFP**, bright ^{1}H MRI signals were observed in both hinder limbs (Figure 5b). The bladder region also showed strong ^{1}H MRI signals, which could be ascribed to the renal clearance of unreacted **NRFP** and GDTy cleaved from **NRFP** (Figure 5b). As revealed by ^{19}F MRI, right hinder limbs showed strong signals, the intensity of which decreased over time, while left hinder limbs did not, indicating the successful *in vivo* imaging of NE. The bladder also exhibited strong signals, the intensity of which increased gradually. This phenomenon could be attributed to the presence of BTFBT that is cleaved from **NRFP** and accumulate in the bladder through renal clearance. There observations are further confirmed with SNR analysis (Figure 5c). To study the specificity of **NRFP** towards NE for *in vivo* imaging, we also subjected some BALB/c mice to MRI, whose left hinder limbs and right hinder limbs were injected with **NRFP** and GSH, and **NRFP** and H_2O_2, respectively (Figure S6). Similar bright ^{1}H MRI signals could be seen in both hinder limbs and the bladder. More importantly, no significant ^{19}F MRI signals were observed for both hinder limbs, indicating the excellent selectivity of **NRFP** towards NE for *in vivo* imaging. These results demonstrate the successful application of **NRFP** for *in vivo* deep-tissue imaging of NE with anatomical details provided by ^{1}H MRI and specific distribution offered by ^{19}F MRI.

Conclusion

In summary, we have developed a small-molecular ^{19}F MRI probe (**NRFP**) by conjugating a fluorine-containing moiety and a paramagnetic Gd chelates *via* a NE-responsive aromatic thiocarbonate linkage, which allows for detection and imaging of NE *via* ^{19}F NMR/MRI. Its capacity and specificity for sensing and imaging NE have been clearly illustrated by a series of *in vitro*, *ex vivo*, and *in vivo* detecting/imaging experiments. It is also noteworthy that **NRFP** and its cleaved products could undergo prompt renal clearance, which significantly minimizes their potential side effects. Though the previously reported fluorescence-based methods have lower detection limits for NE, they are restricted to cellular imaging or *ex vivo* imaging due to the shallow tissue penetration and the interference of *in vivo* autofluorescence.[15–16] In contrast, our work demonstrates a promising means for selective detection and specific imaging of NE, a representative neurotransmitter involved in many biological processes, in deep tissues of living subjects in a noninvasive manner with low background interference. More importantly, the design strategy of this probe could be extended to the development of high-performance probes

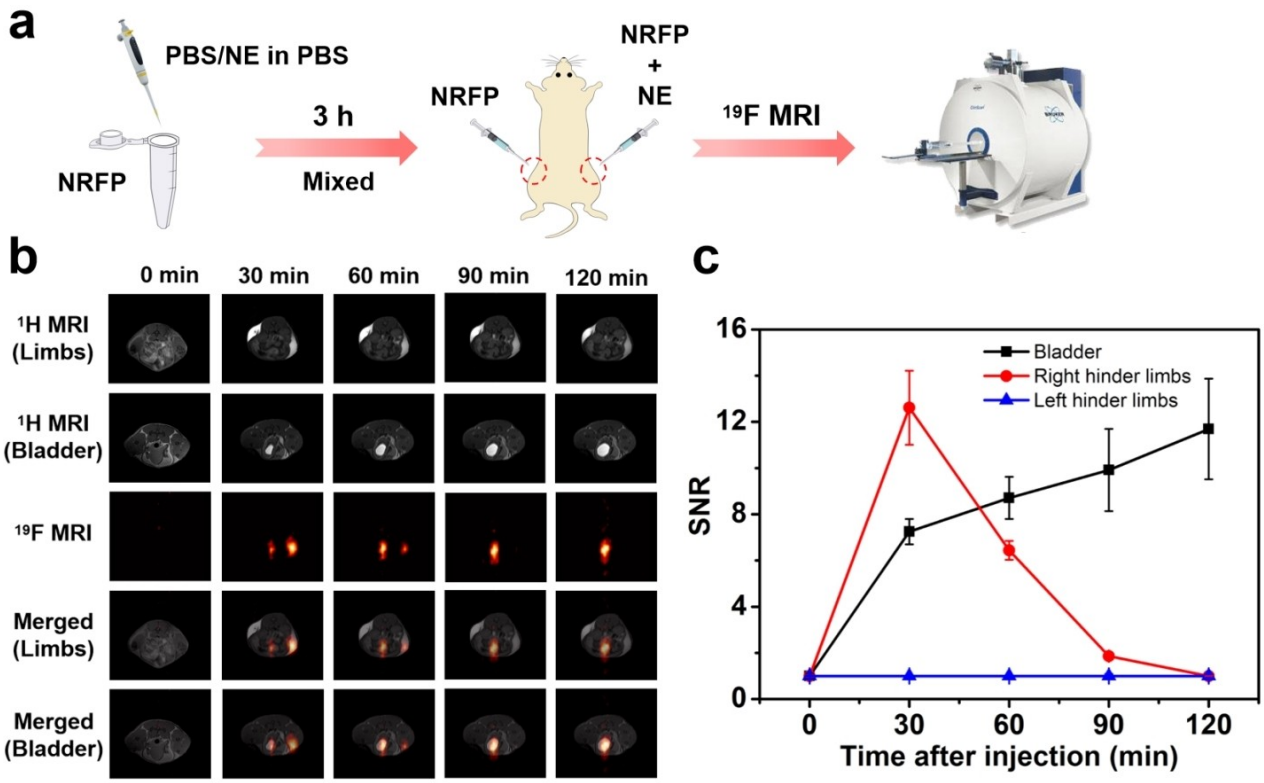

Figure 5. (a) A schematic illustration showing the protocol for *in vivo* ^{19}F MRI. The center frequency corresponding to the ^{19}F chemical shift at −62.7 ppm was chosen for ^{19}F MRI. (b) Representative ^{1}H and ^{19}F MR images of living mice (BALB/c) at pre-injection (0 min) or indicated time points after subcutaneous injection of prepared **NRFP** solution (200 μL), which contains 10 mM **NRFP** in 1 × PBS alone (left hinder limbs) and 10 mM **NRFP** in 1 × PBS incubated with 50 equiv. NE (right hinder limbs) for 3 h. (c) SNR analysis on the results of the experiment as indicated in (b) (n = 3). The average SNR for the left thigh regions of the ^{19}F MR images at 0 min was set as 1.0 and the other SNRs were normalized accordingly.

aiming at sensing and imaging other bioactive species (e.g., biomarkers) in different biological systems.

Experimental Section

Synthesis

All chemicals were purchased commercial sources and used as received without further purification. Unless noted otherwise, all reactions were performed under inert (N_2 or Ar) environments. Please see the Supporting Information for details.

Tri-*tert*-butyl 2,2′,2″-(1,4,7,10-tertraazacyclododecane-1,4,7-triyl)tri-acetate (1, *t*Bu-DO3A)

1, **2**, and **3** were synthesized according to a previous report by our group.[32] Briefly, cyclen (10.336 g, 60.0 mmol) and anhydrous sodium acetate (14.765 g, 180.0 mmol, 3.0 equiv.) were dissolved in 180.0 mL *N*,*N*-dimethylacetamide (DMA). A solution of *tert*-butyl bromoacetate (35.110 g, 29.1 mL, 180.0 mmol, 3.0 equiv.) in 40.0 mL DMA was added dropwise to the mixture. After vigorously stirred at room temperature (RT) for 48 h, the suspension was quenched by saturated sodium bicarbonate aqueous solution. The resulting mixture was concentrated. The residue was purified by flash chromatography (100% CH_2Cl_2 to 15% *v*/*v* CH_3OH/CH_2Cl_2) on silica gel to give **1** (21.87 g, 42.5 mmol, 71%) as a white powder.

^{1}H NMR (600 MHz, CD_3OD): δ 3.41 (4 H, s), 3.36 (2 H, s), 3.14 (4 H, t, J = 6.5 Hz), 2.98 (4 H, t, J = 6.6 Hz), 2.79 (4 H, t, J = 5.5 Hz), 2.69 (4 H, t, J = 6.5 Hz), 1.48 (9 H, s), 1.48 (18 H, s), the peak for –N*H*– on the ring could not be observed; ^{13}C NMR (151 MHz, CD_3OD): δ 171.18, 81.20, 56.23, 50.37, 49.09, 45.62, 27.03. HR-ESI-MS (m/z) calculated for $C_{26}H_{51}N_4O_6$ $[M+H]^+$: 515.3803, found: 515.3820.

Tri-*tert*-butyl 2,2′,2″-(10-(2-methoxy-2-oxoethyl)-1,4,7,10-tetraazacy-clododecane-1,4,7-triyl)tr-riacetate (2)

1 (6.172 g, 12.5 mmol) and K_2CO_3 (3.455 g, 25.0 mmol, 2 equiv.) were dissolved in 40 mL anhydrous acetonitrile. Subsequently, methyl chloroacetate (2.984 g, 2.40 mL, 27.5 mmol, 2.2 equiv.) was added to the mixture. The suspension was vigorously stirred at room temperature for 12 h. After filtration, the filtrate was concentrated and purified by flash chromatography (100% CH_2Cl_2 to 20% *v*/*v* CH_3OH/CH_2Cl_2) to give **2** (6.412 mg, 10.9 mmol, 87%) as a yellow oil.

HR-ESI-MS (m/z) calculated for $C_{29}H_{55}N_4O_8$ $[M+H]^+$: 587.4014, found: 587.4047.

2-(4,7,10-Tris(2-(*tert*-butoxy)-2-oxoethyl)-1,4,7,10-tetraazacycl-lodo-decan-1-yl)acetic acid (3)

2 (5.864 mg, 10.0 mmol) was dissolved in a solution (45 mL) of NaOH (1.2 g) in dioxane/H_2O (*v*/*v* = 2:1). The mixture was vigorously stirred at 50 °C overnight and concentrated *in vacuo*. The residue was added to 30 mL DI water and extracted with dichloromethane (DCM, 3×60 mL). The organic phases were collected, dried with Na_2SO_4, and concentrated to give **3** (5.372 g, 9.0 mmol, 90%) as a white foamy solid.

HR-ESI-MS (m/z) calculated for $C_{28}H_{53}N_4O_8$ $[M+H]^+$ and $C_{28}H_{52}N_4O_8Na$ $[M+Na]^+$: 573.3858 and 595.3677, found: 573.3873 and 595.3699.

tert-Butyl (4-((((3,5-bis(trifluoromethyl)phenyl)thio)carbonyl)oxy)-phenethyl)carbamate (4)

3,5-Bis(trifluoromethyl)thiophenol (2.462 g, 1.69 mL, 10 mmol) and triphosgene (1.484 g, 5.0 mmol) were dissolved in 20 mL DCM and stirred at 0 °C. Dry pyridine (827 μL, 10 mmol) in 5.0 mL DCM was added dropwise within 15 min. The mixture was stirred vigorously for 1 h and washed with 100 mL ice water. The organic phase was collected and dried with Na_2SO_4. Subsequently, *N*-Boc-tyramine (2.372 g, 10.0 mmol) and Et_3N (2.77 mL, 20.0 mmol) in 30 mL *N*,*N*-dimethylformamide (DMF) were quickly added to the organic phase and the mixture was continuously stirred overnight at RT. The crude product was concentrated and purified by flash chromatography (100% hexane to 15% *v*/*v* EtOAc/hexane) to give **4** (1.92 g, 3.77 mmol, 75%) as an off-white powder.

^{1}H NMR (600 MHz, $CDCl_3$): δ 8.08 (2 H, s), 7.95 (1 H, s), 7.25 (2 H, d, J = 4.2 Hz), 7.15 (2 H, d, J = 4.3 Hz), 4.56 (1 H, br s), 3.38 (2 H, s), 2.82 (2 H, t, J = 6.8 Hz), 1.45 (9 H, s); ^{13}C NMR (151 MHz, $CDCl_3$): δ 166.98, 155.81, 149.60, 137.69, 134.42, 132.91-132.24 (m), 130.69, 129.99, 123.60-123.50 (m), 121.81, 121.05, 79.36, 41.68, 35.63, 28.39; ^{19}F NMR (564 MHz, $CDCl_3$): δ −62.95 (6 F, s). HR-ESI-MS (m/z) calculated for $C_{22}H_{21}F_6NO_4SNa$ $[M+Na]^+$: 532.0988, found: 532.1005.

O-(4-(2-Aminoethyl)phenyl) *S*-(3,5-bis(trifluoromethyl)phenyl) carbonothioate (5)

4 (916 mg, 1.8 mmol) was dissolved in 5 mL of DCM/trifluoroacetic acid (TFA) (v:v = 2:1). The reaction was stirred for 3 h at RT. Once the reaction was completed, the reaction mixture was concentrated *in vacuo* to give crude **5** as a viscous liquid, which was directly used in the next step without further purification.

HR-ESI-MS (m/z) calculated for $C_{17}H_{14}F_6NO_2S$ $[M+H]^+$ and $C_{17}H_{13}F_6NO_2SNa$ $[M+Na]^+$: 410.0644 and 432.4063, found: 410.0667 and 432.4067.

Tri-*tert*-butyl 2,2′,2″-(10-(2-((4-((((3,5-bis(trifluoromethyl)phenyl)-thio)carbonyl)oxy)phenethyl)amino)-2-oxoethyoethyl)-1,4,7,10-tetraaza-cyclododecane-1,4,7-triyl)triacetate (6)

3 (714 mg, 1.2 mmol), EDC·HCl (1.15 g, 5.0 equiv.), NHS (414 mg, 3.0 equiv.) and a catalytic amount of 4-dimethylaminopyridine (DMAP) were dissolved in 40 mL DCM and stirred for 3 h at RT. The resulting mixture was washed with water (30 mL) and saturated saline (30 mL) for two times. The organic phase was collected and dried over Na_2SO_4 to give crude **6** as a yellow liquid, which was directly added to a solution of 20 mL DCM containing crude **5** from last step and a catalytic amount of Et_3N. The mixture was stirred overnight and was concentrated *in vacuo* to give crude **7** as a yellow liquid, which was directly used in the next step without further purification.

HR-ESI-MS (m/z) calculated for $C_{45}H_{63}F_6N_5O_9SNa$ $[M+Na]^+$: 986.4143, found: 986.4151.

2,2′,2′′-(10-(2-((4-((((3,5-Bis(trifluoromethyl)phenyl)thio)carbonyl)-oxy)phenethyl)amino)-2-oxoe-thy-e-thyl)-1,4,7,10-tetraazacyclododecane-1,4,7-triyl)triacetic acid (7, Ligand)

Crude **6** was dissolved in 5 mL trifluoroacetic acid (TFA) and the mixture was stirring at RT for 12 h. The solution was concentrated *in vacuo* to give crude **7** as a yellow viscous liquid, which was directly used in the next step without further purification.

^{19}F NMR (564 MHz, 10% D_2O/H_2O): δ −62.69 (6 F, s). HR-ESI-MS (m/z) calculated for $C_{33}H_{40}F_6N_5O_9S$ $[M+H]^+$ and $C_{33}H_{39}F_6N_5O_9SNa$ $[M+Na]^+$: 796.2445 and 818.2665, found: 796.2449 and 818.2665.

Norepinephrine-responsive ^{19}F MRI Probe (8, NRFP)

Crude **7** was dissolved in 30 mL CH_3OH: H_2O (v:v = 1:1) and $GdCl_3{\cdot}6H_2O$ (1.947 g, 3.0 mmol, 3.0 equiv.) was added. The pH was adjusted to ≈3 with 0.1 M NaOH and the resulting mixture was stirred overnight at 45 °C. The mixture was concentrated *in vacuo*, dissolved in 40 mL CH_3CN and further purified by gradient elution using HPLC (ZORBAX SB-18 column from 2% CH_3CN/98% H_2O to 70% CH_3CN/30% H_2O 0-60 min). The fraction between 24.5-28.0 min was collected. Lyophilization gave **8** (215 mg, 19% from **4**) as an off-while solid.

^{19}F NMR (564 MHz, 10% D_2O/H_2O): δ −62.64 (6 F, br s, decoupled); HR-ESI-MS (m/z) calculated for $C_{33}H_{36}F_6GdN_5O_9SNa$ $[M+Na]^+$: 973.1277, found: 973.1279.

NMR/MRI Instrumentation

All ^{1}H NMR and ^{13}C NMR experiments were carried out on a Bruker AVANCE III HD Ascend spectrometer (600 MHz for ^{1}H, 151 MHz for ^{13}C) with tetramethylsilane as an internal referencing standard. All ^{19}F NMR experiments were carried out on the same instrument (564 MHz for ^{19}F) using a 5 mm BBFO cryoprobe and the spectra were acquired with 18 μs delay and 64 scans. ^{19}F NMR samples were prepared in 10% D_2O/H_2O containing sodium trifluoroacetate (CF_3COONa, chemical shift at −75.4 ppm) as an internal standard. All ^{19}F magnetic resonance imaging (^{19}F MRI) with corresponding ^{1}H MRI were performed on a Bruker BioSpec 94/20 system (400 MHz for ^{1}H and 376 MHz for ^{19}F) equipped with a 40 mm (inner diameter) volume coil. Image acquisition, SNR analysis and pseudocolor rending were carried out with ParaVision 5.1 (Bruker BioSpin).

Preparation of NRFP used for ^{19}F NMR/MRI

The final concentration of **NRFP** in stock solution was determined by ^{19}F NMR using 0.1 mM CF_3COONa as an internal reference. Various analytes were incubated in **NRFP** solutions as indicated and the resulting solutions were subjected to ^{19}F NMR. Among the analytes, $ONOO^-$ was generated by mixing $NaNO_2$ with H_2O_2, and $ROO^\bullet$ was made by dissolving 2,2′-azo-bis(2-amidinopropane)dihydrochloride (AAPH) in water. All other analytes were purchased from commercial sources and used as received.

^{1}H/^{19}F MRI

For acquiring ^{1}H MR images, a RARE sequence was used with the following parameters: T_R/T_E = 1000 ms/8.5 ms, flip angle = 180°, FOV = 4 × 4 cm^2, slice thickness = 1 mm, matrix = 256 × 256, average = 4 (NEX = 4). The total acquisition time for each time point was about 3.2 min.

For acquiring ^{19}F MR images, a RARE sequence was used with the following parameters: T_R/T_E = 800 ms/8.5 ms, flip angle = 180°, FOV = 4 × 4 cm^2, slice thickness = 20 mm, matrix = 32 × 32, average = 196 (NEX = 196). The total acquisition time for each time point was about 15.68 min.

Cell Culturing

L02 cells and HepG2 cells were cultured in Dulbecco's Modified Eagle's Medium (DMEM) supplemented with 10% fetal bovine serum (FBS, Hyclone). All cells were maintained in a humidified atmosphere containing 5% CO_2.

Cytotoxicity Evaluation

3-(4,5-dimethylthiazol-2-yl)-2,5-diphenyltetrazolium bromide (MTT) assays were used for cytotoxicity evaluation. L02 cells and HepG2 were firstly seeded into a 96-well plate at a density of 1×10^4 cells/well and incubated for 24 h. After washed twice with PBS, the cells were incubated with fresh media containing **NRFP** at various concentrations (0, 0.5, 1, 2, 4, 6, 8, 10, 15 and 20 mM) for another 24 h. The concentration of **NRFP** was determined by ICP-MS. Subsequently, the media of each well was replaced with 100 μL of fresh media containing MTT (0.5 mg mL^{-1}) and the plate was incubated for 4 h at 37 °C. Then, the media in each well were replaced with 200 μL DMSO. The absorbance at 490 nm of each well was measured on a MultiSkan FC microplate reader immediately. Cell viabilities were calculated accordingly.

Animal Ethics

Animal experiments were conducted according to the protocols approved by the Institutional Animal Care and Use Committee of Xiamen University.

Ex vivo Imaging of NE by ^{19}F MRI with NRFP

10 mM **NRFP** in 1 × PBS solutions were subcutaneously injected to two spots of a piece of pork. 50 equiv. NE dissolved in PBS was subcutaneously injected into one of the two spots as indicated. Then the pork was subjected to ^{19}F MRI.

In vivo Imaging of NE *via* ^{19}F MRI with NRFP

10 mM **NRFP** in 1 × PBS buffer (pH 7.4) were incubated alone or together with 50 equiv. analytes (NE, GSH or H_2O_2) for 3 h. Then, the solutions were subcutaneously injected into the hinder limbs of BALB/c mice as indicated. Then the mice were subjected to ^{19}F MRI.

Acknowledgements

This work was partially supported by the National Natural Science Foundation of China (22125702, 22077107, and 92059109), the Natural Science Foundation of Fujian Province of China (2020J02001), and the Youth Innovation Funding Program of Xiamen City (3502Z20206051).

Conflict of Interest

The authors declare no conflict of interest.

Data Availability Statement

The data that support the findings of this study are available in the supplementary material of this article.

Keywords: ^{19}F NMR/MRI · deep-tissue sensing · imaging agents · *in vivo* imaging · norepinephrine

[1] S. D. Robertson, N. W. Plummer, J. de Marchena, P. Jensen, *Nat. Neurosci.* **2013**, *16*, 1016–1023.
[2] Y. U. Liu, Y. L. Ying, Y. J. Li, U. B. Eyo, T. J. Chen, J. Y. Zheng, A. D. Umpierre, J. Zhu, D. B. Bosco, H. L. Dong, L. J. Wu, *Nat. Neurosci.* **2019**, *22*, 1771–1781.
[3] D. J. Richards, Y. Li, C. M. Kerr, J. Yao, G. C. Beeson, R. C. Coyle, X. Chen, J. Jia, B. Damon, R. Wilson, E. S. Hazard, G. Hardiman, D. R. Menick, C. C. Beeson, H. Yao, T. Ye, Y. Mei, *Nat. Biomed. Eng.* **2020**, *4*, 446–462.
[4] L. A. Schwarz, K. Miyamichi, X. J. J. Gao, K. T. Beier, B. Weissbourd, K. E. DeLoach, J. Ren, S. Ibanes, R. C. Malenka, E. J. Kremer, L. Q. Luo, *Nature* **2015**, *524*, 88.
[5] A. H. Zahalka, A. Arnal-Estape, M. Maryanovich, F. Nakahara, C. D. Cruz, L. W. S. Finley, P. S. Frenette, *Science* **2017**, *358*, 321–326.
[6] H. I. L. Jacobs, J. M. Riphagen, I. Ramakers, F. R. J. Verhey, *Mol. Psychiatry* **2021**, *26*, 897–906.
[7] W. W. Xue, F. Y. Yang, P. P. Wang, G. X. Zheng, Y. Z. Chen, X. J. Yao, F. Zhu, *ACS Chem. Neurosci.* **2018**, *9*, 1128–1140.
[8] C. G. Abdallah, L. A. Averill, J. H. Krystal, S. M. Southwick, A. F. Arnsten, *Behav. Brain Sci.* **2016**, *39*, e201.
[9] G. H. Diering, R. S. Nirujogi, R. H. Roth, P. F. Worley, A. Pandey, R. L. Huganir, *Science* **2017**, *355*, 511–515.
[10] M. J. Betts, E. Kirilina, M. C. G. Otaduy, D. Ivanov, J. Acosta-Cabronero, M. F. Callaghan, C. Lambert, A. Cardenas-Blanco, K. Pine, L. Passamonti, C. Loane, M. C. Keuken, P. Trujillo, F. Lusebrink, H. Mattern, K. Y. Liu, N. Priovoulos, K. Fliessbach, M. J. Dahl, A. Maass, C. F. Madelung, D. Meder, A. J. Ehrenberg, O. Speck, N. Weiskopf, R. Dolan, B. Inglis, D. Tosun, M. Morawski, F. A. Zucca, H. R. Siebner, M. Mather, K. Uludag, H. Heinsen, B. A. Poser, R. Howard, L. Zecca, J. B. Rowe, L. T. Grinberg, H. I. L. Jacobs, E. Duzel, D. Hammerer, *Brain* **2019**, *142*, 2558–2571.
[11] S. Moriguchi, M. Yamada, H. Takano, T. Nagashima, K. Takahata, K. Yokokawa, T. Ito, T. Ishii, Y. Kimura, M. R. Zhang, M. Mimura, T. Suhara, *Am. J. Psychiat.* **2017**, *174*, 36–41.
[12] J. Feng, C. M. Zhang, J. E. Lischinsky, M. Jing, J. H. Zhou, H. Wang, Y. J. Zhang, A. Dong, Z. F. Wu, H. Wu, W. Y. Chen, P. Zhang, J. Zou, S. A. Hires, J. J. Zhu, G. H. Cui, D. Y. Lin, J. L. Du, Y. L. Li, *Neuron* **2019**, *102*, 745–761.
[13] M. Dunn, A. Henke, S. Clark, Y. Kovalyova, K. A. Kempadoo, R. J. Karpowicz, Jr., E. R. Kandel, D. Sulzer, D. Sames, *Nat. Commun.* **2018**, *9*, 2838.
[14] J. An, Y. Shi, J. Fang, Y. Hu, Y. Liu, *Chem. Eng. J.* **2021**, *425*, 130595.
[15] L. Zhang, X. A. Liu, K. D. Gillis, T. E. Glass, *Angew. Chem. Int. Ed.* **2019**, *58*, 7611–7614; *Angew. Chem.* **2019**, *131*, 7693–7696.
[16] N. Zhou, F. Huo, Y. Yue, C. Yin, *J. Am. Chem. Soc.* **2020**, *142*, 17751–17755.
[17] M. Carril, *J. Mater. Chem. B* **2017**, *5*, 4332–4347.
[18] Z. H. Zhao, Z. J. Zhou, J. F. Bao, Z. Y. Wang, J. Hu, X. Q. Chi, K. Y. Ni, R. F. Wang, X. Y. Chen, Z. Chen, J. H. Gao, *Nat. Commun.* **2013**, *4*, 2266.
[19] Z. J. Zhou, L. J. Yang, J. H. Gao, X. Y. Chen, *Adv. Mater.* **2019**, *31*, 1804567.
[20] L. J. Yang, Z. Y. Wang, L. C. Ma, A. Li, J. Y. Xin, R. X. Wei, H. Y. Lin, R. F. Wang, Z. Chen, J. H. Gao, *ACS Nano* **2018**, *12*, 4605–4614.
[21] C. J. Sun, H. Y. Lin, X. Q. Gong, Z. X. Yang, Y. Mo, X. Y. Chen, J. H. Gao, *J. Am. Chem. Soc.* **2020**, *142*, 198–206.
[22] Z. X. Yang, H. Y. Lin, J. Q. Huang, A. Li, C. J. Sun, J. Richmond, J. H. Gao, *Chem. Commun.* **2019**, *55*, 4546–4549.
[23] L. N. Carter, O. Addison, N. Naji, P. Seres, A. H. Wilman, D. E. T. Shepherd, L. Grover, S. Cox, *Acta Biomater.* **2020**, *107*, 338–348.
[24] J. Wahsner, E. M. Gale, A. Rodriguez-Rodriguez, P. Caravan, *Chem. Rev.* **2019**, *119*, 957–1057.
[25] I. Tirotta, V. Dichiarante, C. Pigliacelli, G. Cavallo, G. Terraneo, F. B. Bombelli, P. Metrangolo, G. Resnati, *Chem. Rev.* **2015**, *115*, 1106–1129.
[26] C. Zhang, K. Yan, C. Fu, H. Peng, C. J. Hawker, A. K. Whittaker, *Chem. Rev.* **2022**, *122*, 167–208.
[27] H. Zhang, S. Chen, Y. Yuan, Y. Li, Z. Jiang, X. Zhou, *ACS Appl. Bio Mater.* **2019**, *2*, 27–32.
[28] M. Cametti, B. Crousse, P. Metrangolo, R. Milani, G. Resnati, *Chem. Soc. Rev.* **2012**, *41*, 31–42.
[29] C. Zhang, S. S. Moonshi, W. Q. Wang, H. T. Ta, Y. X. Han, F. Y. Han, H. Peng, P. Kral, B. E. Rolfe, J. J. Gooding, K. Gaus, A. K. Whittaker, *ACS Nano* **2018**, *12*, 9162–9176.
[30] A. A. Kislukhin, H. Y. Xu, S. R. Adams, K. H. Narsinh, R. Y. Tsien, E. T. Ahrens, *Nat. Mater.* **2016**, *15*, 662–668.
[31] A. Li, L. X. Li, X. Liu, D. X. Chen, Y. F. Fan, H. Y. Lin, J. H. Gao, *Chem. Commun.* **2021**, *57*, 9622–9625.
[32] A. Li, X. X. Tang, X. Q. Gong, H. M. Chen, H. Y. Lin, J. H. Gao, *Chem. Commun.* **2019**, *55*, 12455–12458.
[33] H. Y. Lin, X. X. Tang, A. Li, J. H. Gao, *Adv. Mater.* **2021**, *2005657*.
[34] X. X. Tang, X. Q. Gong, A. Li, H. Y. Lin, C. Y. Peng, X. Z. Zhang, X. Y. Chen, J. H. Gao, *Nano Lett.* **2020**, *20*, 363–371.
[35] C. Wang, S. R. Adams, E. T. Ahrens, *Acc. Chem. Res.* **2021**, *54*, 3060–3070.
[36] X. L. Zhu, X. X. Tang, H. Y. Lin, S. G. Shi, H. H. Xiong, Q. J. Zhou, A. Li, Q. Y. Wang, X. Y. Chen, J. H. Gao, *Chem* **2020**, *6*, 1134–1148.
[37] K. Akazawa, F. Sugihara, T. Nakamura, H. Matsushita, H. Mukai, R. Akimoto, M. Minoshima, S. Mizukami, K. Kikuchi, *Angew. Chem. Int. Ed.* **2018**, *57*, 16742–16747; *Angew. Chem.* **2018**, *130*, 16984–16989.
[38] I. Ashur, H. Allouche-Arnon, A. Bar-Shir, *Angew. Chem. Int. Ed.* **2018**, *57*, 7478–7482; *Angew. Chem.* **2018**, *130*, 7600–7604.
[39] Z. L. Ding, H. B. Sun, S. C. Ge, Y. Cai, Y. Yuan, Z. J. Hai, T. X. Tao, J. M. Hu, B. Hu, J. F. Wang, G. L. Liang, *Adv. Funct. Mater.* **2019**, *29*, 1903860.
[40] C. K. Fu, B. Demir, S. Alcantara, V. Kumar, F. Han, H. G. Kelly, X. Tan, Y. Yu, W. Z. Xu, J. C. Zhao, C. Zhang, H. Peng, C. Boyer, T. M. Woodruff, S. J. Kent, D. J. Searles, A. K. Whittaker, *Angew. Chem. Int. Ed.* **2020**, *59*, 4729–4735; *Angew. Chem.* **2020**, *132*, 4759–4765.
[41] C. Guo, S. Y. Xu, A. Arshad, L. Y. Wang, *Chem. Commun.* **2018**, *54*, 9853–9856.
[42] P. Huang, W. Guo, G. Yang, H. Song, Y. Wang, C. Wang, D. Kong, W. Wang, *ACS Appl. Mater. Interfaces* **2018**, *10*, 18532–18542.
[43] A. H. Jahromi, C. Wang, S. R. Adams, W. L. Zhu, K. Narsinh, H. Y. Xu, D. L. Gray, R. Y. Tsien, E. T. Ahrens, *ACS Nano* **2019**, *13*, 143–151.
[44] Y. W. Li, H. C. Zhang, C. Guo, G. F. Hu, L. Y. Wang, *Anal. Chem.* **2020**, *92*, 11739–11746.
[45] Y. Yuan, S. C. Ge, H. B. Sun, X. J. Dong, H. X. Zhao, L. N. An, J. Zhang, J. F. Wang, B. Hu, G. L. Liang, *ACS Nano* **2015**, *9*, 5117–5124.
[46] A. Li, X. Luo, L. Li, D. Chen, X. Liu, Z. Yang, L. Yang, J. Gao, H. Lin, *Anal. Chem.* **2021**, *93*, 16552–16561.
[47] X. X. Tang, X. Q. Gong, J. Ming, D. X. Chen, H. Y. Lin, J. H. Gao, *Anal. Chem.* **2020**, *92*, 16293–16300.
[48] R. Pujales-Paradela, T. Savic, P. Perez-Lourido, D. Esteban-Gomez, G. Angelovski, M. Botta, C. Platas-Iglesias, *Inorg. Chem.* **2019**, *58*, 7571–7583.
[49] S. Mizukami, R. Takikawa, F. Sugihara, Y. Hori, H. Tochio, M. Walchli, M. Shirakawa, K. Kikuchi, *J. Am. Chem. Soc.* **2008**, *130*, 794–795.
[50] D. Xie, M. Yu, R. T. Kadakia, E. L. Que, *Acc. Chem. Res.* **2020**, *53*, 2–10.

Manuscript received: May 9, 2022
Revised manuscript received: June 8, 2022